JACS Au
AN OPEN ACCESS JOURNAL OF THE AMERICAN CHEMICAL SOCIETY

pubs.acs.org/jacsau
Article

Tuning Chemical Interface Damping: Competition between Surface Damping Pathways in Amalgamated Gold Nanorods Coated with Mesoporous Silica Shells

Yola Yolanda Alizar, Mukunthan Ramasamy, Geun Wan Kim, and Ji Won Ha*

Cite This: JACS Au 2023, 3, 3247−3258
Read Online

ACCESS | Metrics & More | Article Recommendations | Supporting Information

ABSTRACT: The mechanism of mercury (Hg) amalgamation in gold nanorods coated with a mesoporous silica shell (AuNRs@mSiO$_2$) and the effect of chemical treatments on the localized surface plasmon resonance (LSPR) spectral changes in single amalgamated AuNRs@mSiO$_2$ remains unclear. In this study, we investigated Hg amalgamation and inward Hg diffusion in single AuNRs@mSiO$_2$ without structural deformation via dark-field scattering spectroscopy and X-ray photoelectron spectroscopy. Then, we investigated the chemisorption of thiol molecules on single amalgamated AuNRs@Hg-mSiO$_2$. Unlike previous studies on single AuNRs, the thiolation on single AuNRs@Hg-mSiO$_2$ resulted in a redshift and line width narrowing of the LSPR peak within 1 h. To determine the chemical effect, we investigated the competition between two surface damping pathways: metal interface damping (MID) and chemical interface damping (CID). When we exposed amalgamated AuNRs@Hg-mSiO$_2$ to 1-alkanethiols with three different carbon chain lengths for 1 h, we observed an increase in the line width broadening with longer chain lengths owing to enhanced CID, demonstrating the tunability of CID and LSPR properties upon chemical treatments. We also investigated the competition between the two surface damping pathways as a function of the time-dependent Au−Hg surface properties in AuNRs@Hg-mSiO$_2$. The 24-h Hg treatment resulted in increased line width broadening compared to the 1-h treatment for the same thiols, which was attributed to the predominance of CID. This was in contrast to the predominance of MID under the 1-h treatment, which formed a core−shell structure. Therefore, this study provides new insights into the Hg amalgamation process, the effect of chemical treatments, competition between surface decay pathways, and LSPR control in AuNRs@mSiO$_2$.

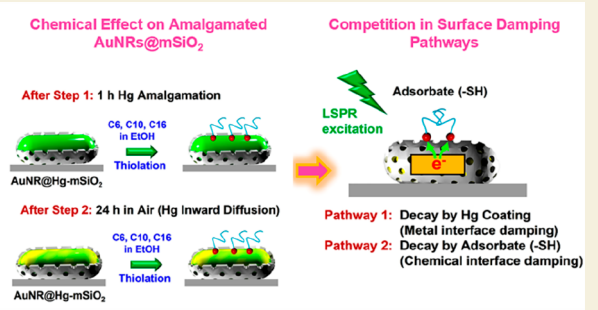

KEYWORDS: *Hg amalgamation, chemical interface damping, plasmon decay, localized surface plasmon resonance, gold nanorods*

INTRODUCTION

Mercury (Hg) is a highly toxic pollutant among the other heavy metals in air, water, and soil.[1−4] The most stable inorganic form of Hg is the divalent ion (Hg^{2+}), which is widely distributed in the ecosystem.[3,5] Hg^{2+} is water-soluble, nonbiodegradable, and highly reactive, causing severe health problems even at the lowest concentration that accumulates in living organisms through the food chain.[6,7] Several methods have been successfully used to detect and determine Hg^{2+}.[1−3,5−8] In these methods, plasmonic nanoparticles (NPs), such as gold nanoparticles (AuNPs), have been widely used for Hg detection and purification by probing the changes in the optical properties of AuNPs owing to their strong interaction with Hg.[9,10]

The strong affinity between Au and Hg results in nanoscale amalgams when AuNPs are exposed to Hg ions. Dark-field (DF) scattering microscopy and spectroscopy have been used as robust techniques to investigate the localized surface plasmon resonance (LSPR) spectral change owing to Au−Hg interactions during the amalgamation process at the single-particle level.[11,12] For example, Schopf et al. used DF microscopy and spectroscopy to investigate the morphological and spectral changes in single gold nanorods (AuNRs) caused by Au−Hg amalgam formation.[11] We previously described the Hg amalgamation process, which resulted in structural changes and a blueshift in the LSPR spectrum of bare AuNRs at the single-particle level.[13] Hence, the morphological changes resulting from Hg amalgamation altered the LSPR properties of the AuNRs. Furthermore, Mertens et al. showed that Hg atoms could adsorb onto NP surfaces and form Hg layers, a core−shell structure. Then, Hg atoms slowly diffuse into Au atoms and form Au−Hg nanoalloys in air.[14]

Received: September 29, 2023
Revised: October 24, 2023
Accepted: October 30, 2023
Published: November 13, 2023

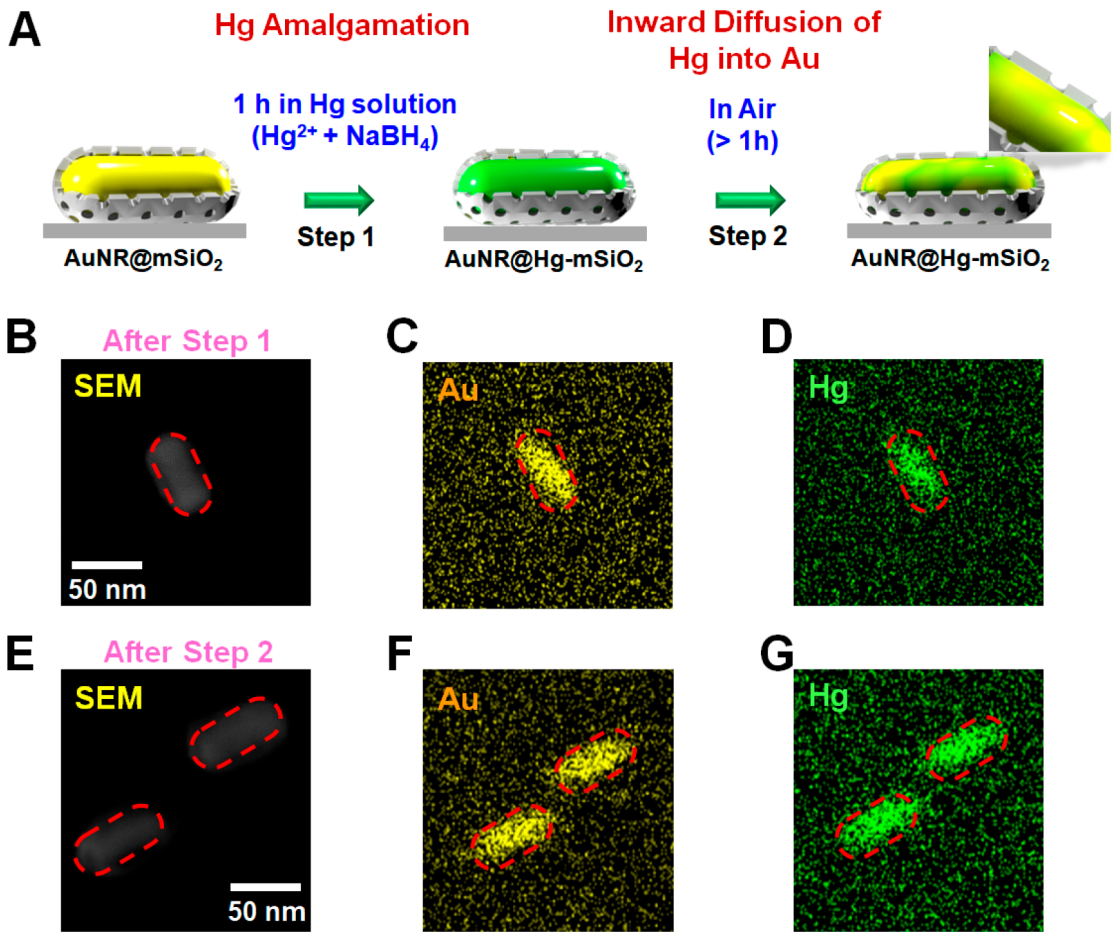

Figure 1. (A) Schematic representation of the Hg amalgamation and thiolation processes in AuNRs@mSiO$_2$. In step 1, the Au−Hg core−shell nanoparticle (NP) formed in the Hg amalgamation solution. In step 2, inward diffusion of Hg into the AuNR can occur after the NP is removed from the Hg solution. (B−D) SEM and EDX elemental mapping images of Au and Hg in the amalgamated AuNRs@mSiO$_2$ after step 1. (E−G) SEM and EDX elemental mapping images of Au and Hg in the amalgamated AuNRs@mSiO$_2$ after step 2.

Recently, we studied the spectral changes caused by Hg amalgamation without structural deformation in single AuNRs coated with mesoporous silica (AuNRs@mSiO$_2$).[15] When we exposed the amalgamated AuNRs@mSiO$_2$ to air for a long time, the inward Hg diffusion into the AuNR core resulted in a gradual redshift and line width narrowing of the LSPR peak.[15] Moreover, the dielectric silica coating provided structural stability to the AuNR core against electrochemical manipulations.[16] However, further studies are needed to better understand the Au−Hg interaction mechanism and associated LSPR changes in amalgamated AuNRs@mSiO$_2$ upon exposure to chemical environments. To the best of our knowledge, no studies have reported on amalgamated AuNRs@mSiO$_2$ exposed to adsorbate molecules that may promote changes in the LSPR properties of the single NPs. Furthermore, chemical interface damping (CID),[17−23] one of the plasmon decay pathways in plasmonic NPs, and its competition with other surface damping pathways in amalgamated AuNRs@mSiO$_2$ remain largely unstudied.

In this study, DF spectroscopy and X-ray photoelectron spectroscopy (XPS) were used to investigate the mechanism of Hg amalgamation and Hg inner diffusion into AuNRs@mSiO$_2$ without a structural transformation. Additionally, we investigated the LSPR spectral variations and CID effects caused by the chemisorption of thiol molecules with different carbon chain lengths on amalgamated AuNRs@mSiO$_2$. An effective method for tuning the LSPR properties by chemical treatment was demonstrated in amalgamated AuNRs@mSiO$_2$, and the competition between the two surface decay pathways was investigated.

EXPERIMENTAL METHODS

Chemicals and Materials

Mercury(II) chloride ($HgCl_2$, ≥99.5%) and sodium borohydride ($NaBH_4$, ≥98%) were purchased from Sigma−Aldrich (St. Louis, MO, USA) and used without further purification. We purchased AuNRs@mSiO$_2$ from Nanopartz (Loveland, CO, USA). All thiol molecules (1-hexanethiol, 1-decanethiol, and 1-hexadecanethiol) were purchased from Sigma−Aldrich (St. Louis, MO, USA). The thiol solution was diluted with ethanol.

Sample Preparation

To prevent aggregation and maintain a proper concentration of NPs on the substrate surface, colloidal solutions of AuNRs@mSiO$_2$ were diluted to the necessary concentration with 18.2-MΩ pure distilled water and sonicated for 15 min. The samples were prepared by spin-casting a diluted AuNRs@mSiO$_2$ solution onto a precleaned (ultrasonically in ethanol, distilled water, and 2-propanol for 15 min each) glass slide and drying it. Then, the samples were exposed to Hg amalgamation solution for 1 h (step 1), and exposure was continued in air for 24 h (step 2). For the single-particle scattering microscopy and spectroscopy studies, a 22 mm × 22 mm no. 1.5 coverslip (Corning, NY) was placed on the glass slide. To investigate the NPs at the single-particle level and minimize the interparticle LSPR

https://doi.org/10.1021/jacsau.3c00578
JACS Au 2023, 3, 3247−3258

coupling, the NP concentration on the slide glass surface was held constant at 1 μm^{-2}.

Structural Characterization

Scanning electron microscopy (SEM, JSM-6500F, JEOL, Japan) and transmission electron microscopy (TEM, JEL-2100F, JEOL, Japan) were used to characterize AuNRs@mSiO$_2$ before and after Hg amalgamation. The lengths and widths of AuNRs@mSiO$_2$ before and after Hg amalgamation were determined in the SEM images, and the structural changes were investigated. Furthermore, by using SEM and energy-dispersive X-ray spectroscopy (EDX), elemental mapping images of amalgamated AuNRs@mSiO$_2$ were obtained.

X-ray Photoelectron Spectroscopy Measurements

XPS data were collected on an XPS system (Thermo Fisher K-alpha) to confirm the state of Hg deposited on the Au surface and the inward diffusion of Hg. The XPS data at high resolution were obtained using an analyzer pass energy of 50.0 eV. The C 1s peak was used as the internal standard for peak positioning.

DF Scattering Microscopy

An inverted Nikon microscope (Nikon Eclipse Ti-2) was used to obtain the DF microscopy images. The microscope used a Nikon Plan Fluor 100 × 0.5−1.3 oil iris objective (NA = 0.7−1.4) and an inverted Nikon DF condenser (NA = 0.7−1.4) in the DF mode. An Andor iXon EMCCD camera (iXon Ultra 897) was used to capture detailed DF scattering images of the desired NPs. The collected images were analyzed by using ImageJ and MATLAB.

Single-Particle DF Scattering Spectroscopy

The DF scattering spectra of single AuNRs@mSiO$_2$ and amalgamated AuNRs@Hg-mSiO$_2$ were acquired by using an Andor spectrophotometer (Shamrock 303i, SR-303I-A, UK) connected to an Andor charge-coupled device (CCD) camera (Newton DU920P-OE). The single-particle scattering spectrum was acquired by shifting the scanning stage to the appropriate sample location, allowing the objective to gather only the scattered light from the selected NP. The scattered light from a single NP was directed to the spectrophotometer, where it was dispersed using a grating (300 l/mm) and detected by a Newton CCD camera. The background was measured in a particle-free environment. Data analysis was performed using custom-made MATLAB scripts.

RESULTS AND DISCUSSION

Hg Amalgamation and Inward Diffusion in AuNRs@mSiO$_2$ without Structural Deformation

Figure S1 shows an SEM image of AuNRs@mSiO$_2$. Using this image, we determined that the average dimensions of AuNRs@mSiO$_2$ were 54.53(±5.63) nm × 100.7(±8.68) nm with an aspect ratio (AR) of 1.85, as shown in Figure S2. The mesoporous silica shell has a thickness of 18 nm (Figure S3). Figure S4 shows the ultraviolet−visible−near-infrared (UV−vis−NIR) extinction spectrum of AuNRs@mSiO$_2$ in distilled water, and the distinctive transverse and longitudinal LSPR peaks of AuNRs@mSiO$_2$ were at approximately 516 and 693 nm, respectively.

Hg amalgamation in AuNRs@mSiO$_2$ spin-casted on a precleaned glass slide was then achieved (Figure 1A).[13,15] The mesoporous silica shell surrounding the AuNRs prevented the nanoparticles from aggregating upon deposition on the slide.[13,15,24] The AuNRs@mSiO$_2$ were exposed to a solution containing a high concentration of 10 μM $HgCl_2$ and 10 mM $NaBH_4$, as shown in Figure 1A (step 1).[13,15] Because of its strong reducing ability, $NaBH_4$ was used to reduce Hg(II) ions to Hg(0).[25] The Hg ions initially adsorbed on the AuNR surface, followed by the formation of a Hg layer owing to the strong affinity between Au and Hg. The Hg surface layer facilitates the formation of the Au−Hg alloy.[25] Owing to the low Hg cohesive energy (0.67 eV/atom) compared to that of Au (3.81 eV/atom), Au−Hg alloy formation is facilitated by dissolution and diffusion of Au atom into the Au/Hg interface or Hg layer.[12,13,15] Furthermore, the formation of the Au−Hg alloy via diffusion results in the structural transformation of bare AuNRs owing to the gradual increase in the Hg content in AuNRs. However, in AuNRs@mSiO$_2$, the SiO$_2$ shell provided structural stability to the AuNR core; thus, no noticeable structural transformation was observed after Hg amalgamation, as shown in the SEM image (Figure S5A). The average aspect ratio (AR) was approximately 1.78, corresponding to a 59.20(±5.53)-nm width and 105.45(±8.2)-nm length (Figure S5B). Moreover, the inward Hg diffusion (a few nanometers) into the AuNR core, a slow process that requires >24 h, then occurred in air (Figure 1A, step 2).[15]

To further confirm the Hg amalgamation and inward Hg diffusion into AuNRs@mSiO$_2$, field-emission SEM (FE-SEM) with EDX elemental analysis and XPS measurements were performed. The EDX elemental mapping images showed that Au and Hg were distributed along the AuNRs inside the mesoporous silica shell after amalgamation in steps 1 and 2 (Figure 1B−G). Additional EDX data of the amalgamated AuNRs@mSiO$_2$ are provided in Figure S6. We used high-resolution XPS to characterize the surface state of the amalgamated AuNRs@mSiO$_2$ after steps 1 and 2 and to clarify the inward diffusion of Hg in step 2 (Figure 1A). As shown in Figures 2 and S7, we analyzed the high-resolution

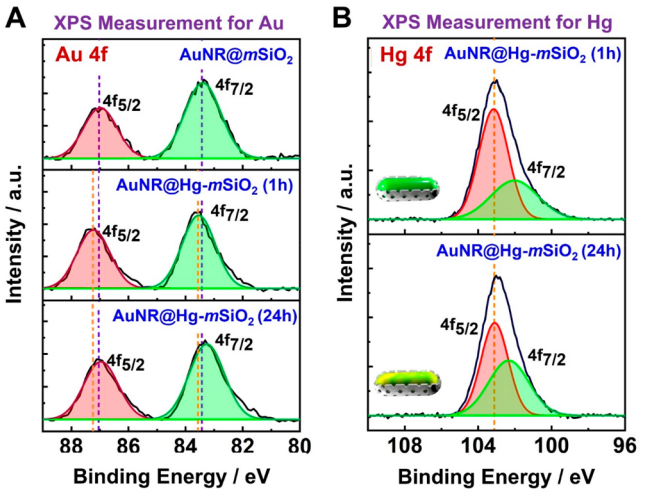

Figure 2. (A) XPS peaks of Au 4f for AuNRs@mSiO$_2$, AuNRs@Hg-mSiO$_2$ (1 h, after step 1), and AuNRs@Hg-mSiO$_2$ (24 h, after step 2). (B) XPS peaks of Hg 4f for AuNRs@mSiO$_2$, AuNRs@Hg-mSiO$_2$ (1 h), and AuNRs@Hg-mSiO$_2$ (24 h)

XPS spectra for Au 4f, Hg 4f, Si 2p, and O 1s at different stages of the experiment, namely, bare AuNRs@mSiO$_2$, amalgamated AuNRs@Hg-mSiO$_2$ for 1 h (step 1), and amalgamated AuNRs@Hg-mSiO$_2$ for 24 h (step 2). From the XPS measurements, two peaks in the Au 4f spectra appear at binding energies of 83.04 and 87.00 eV, respectively, indicating Au $4f_{7/2}$ and Au $4f_{5/2}$ spin−orbital coupling of elemental Au^0 before the Hg treatment (Figure 2A).[26] However, during the initial 1 h of Hg amalgamation (step 1), Hg atoms began interacting with surface atoms of Au and formed a densely packed layer of Hg over the Au surface, forming an Au−Hg core−shell structure. Because the free electron density of Au is higher than that of Hg, electron transfer from Au to Hg is

https://doi.org/10.1021/jacsau.3c00578
JACS Au 2023, 3, 3247−3258

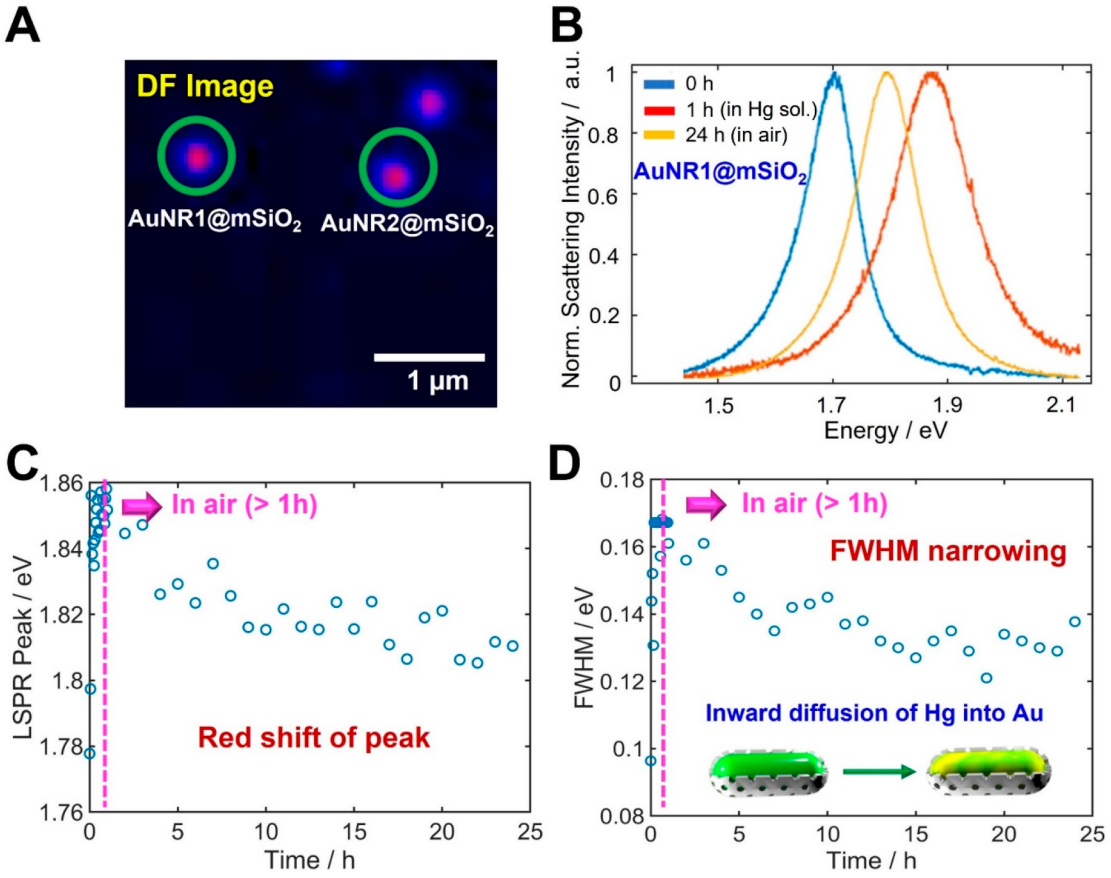

Figure 3. (A) DF scattering image of single AuNR@mSiO$_2$. (B) Normalized scattering spectra of AuNR1@mSiO$_2$ before exposure to Hg solution (blue curve), AuNR1@mSiO$_2$ after exposure to Hg solution for 1 h (red curve), and AuNR1@mSiO$_2$ in air for 24 h (yellow curve). (C) Change in the LSPR peak of AuNR1@mSiO$_2$ (in Figure 2A) exposed to Hg solution as a function of time. After 1 h, AuNR1@mSiO$_2$ was exposed to air and measured at intervals of 1 h. (D) Change in the corresponding LSPR line width of AuNR1@mSiO$_2$ as a function of time.

expected to decrease the electron density of Au at the surface. This decrease in the electron density leads to positively charged Au as shown by the Au 4f spectral shift (Figure 2A) to a higher binding energy (blueshift). Furthermore, after step 1, the amalgamated AuNRs@Hg-mSiO$_2$ (1 h) showed adjacent 4f$_{7/2}$ and 4f$_{5/2}$ peaks in the Hg 4f spectrum, with the peaks resulting from adsorption of Hg atoms on the surface of the AuNRs (Figure 1B and D). In addition, after 24 h of Hg treatment in air (step 2), a solid amalgam of Au−Hg may have formed predominantly (the unamalgamated part of the Au core may have remained), where the Au and Hg atoms were intermixed. Thus, the Au 4f and Hg 4f peaks shifted to lower binding energies compared to those for 1 h of Hg amalgamation. Notably, the XPS peaks for Au shifted back to the locations of those of bare AuNR@mSiO$_2$ before Hg treatment. Therefore, using XPS, we confirmed the formation of the Au−Hg core−shell on the surface of AuNR@mSiO$_2$ at step 1 and the slow Hg inward diffusion and solid Hg−Au amalgam formation after step 2, as depicted in Figure 1A.[14,15,27,28] Further details of the change in work function (Φ) at the different stages of Hg amalgamation of AuNR@mSiO$_2$ are discussed below.

Effects of Hg Amalgamation and Inward Hg Diffusion on the LSPR Properties in Single AuNRs@mSiO$_2$

We investigated the time-dependent LSPR spectral variations caused by Hg amalgamation and inward Hg diffusion in the AuNRs@mSiO$_2$. Figures S8 and S9 show the experimental setup for single-particle DF microscopy and spectroscopy. Figure 3A shows an DF image of AuNRs@mSiO$_2$ immobilized on a glass slide. According to the homogeneous LSPR spectra of AuNRs@mSiO$_2$ exposed to Hg solution, the formation of the Hg metal shell causes a change in the refractive index of the outer surface of the AuNR and thus changes the free electron density of the core metal.[29] Therefore, the higher electron density owing to the formation of the Au−Hg core−shell structure caused the blueshift and line width broadening in the LSPR spectrum after step 1.[13,15] Besides that, the difference in the dielectric function of Au and Hg and the variation in effective dielectric function due to the formation of the Au−Hg core−shell structure may also result in a variation in the LSPR spectrum.[30,31] Since the dielectric function or relative permittivity of plasmonic materials is highly dependent on the surface electron density, a large change in the electron density of states (DOS) at the amalgamated AuNR cores will also contribute to the LSPR shifts in this system.[29−31] The blueshift and line width broadening saturated within 1 h owing to the Hg layer formation at the AuNR surface (Figure 3B−D). Furthermore, the LSPR scattering spectrum was measured for a longer time (every 1 for 24 h) for the AuNRs@mSiO$_2$ after they were removed from the Hg solution and kept in air. The normalized scattering spectra of amalgamated AuNR1@Hg-mSiO$_2$ (marked by the green circle as AuNR1@mSiO$_2$ in Figure 3A) after 1 h in Hg solution and 24 h in air (Figure 3B) show a notable redshift of the LSPR peak. The gradual redshift

https://doi.org/10.1021/jacsau.3c00578
JACS Au 2023, 3, 3247−3258

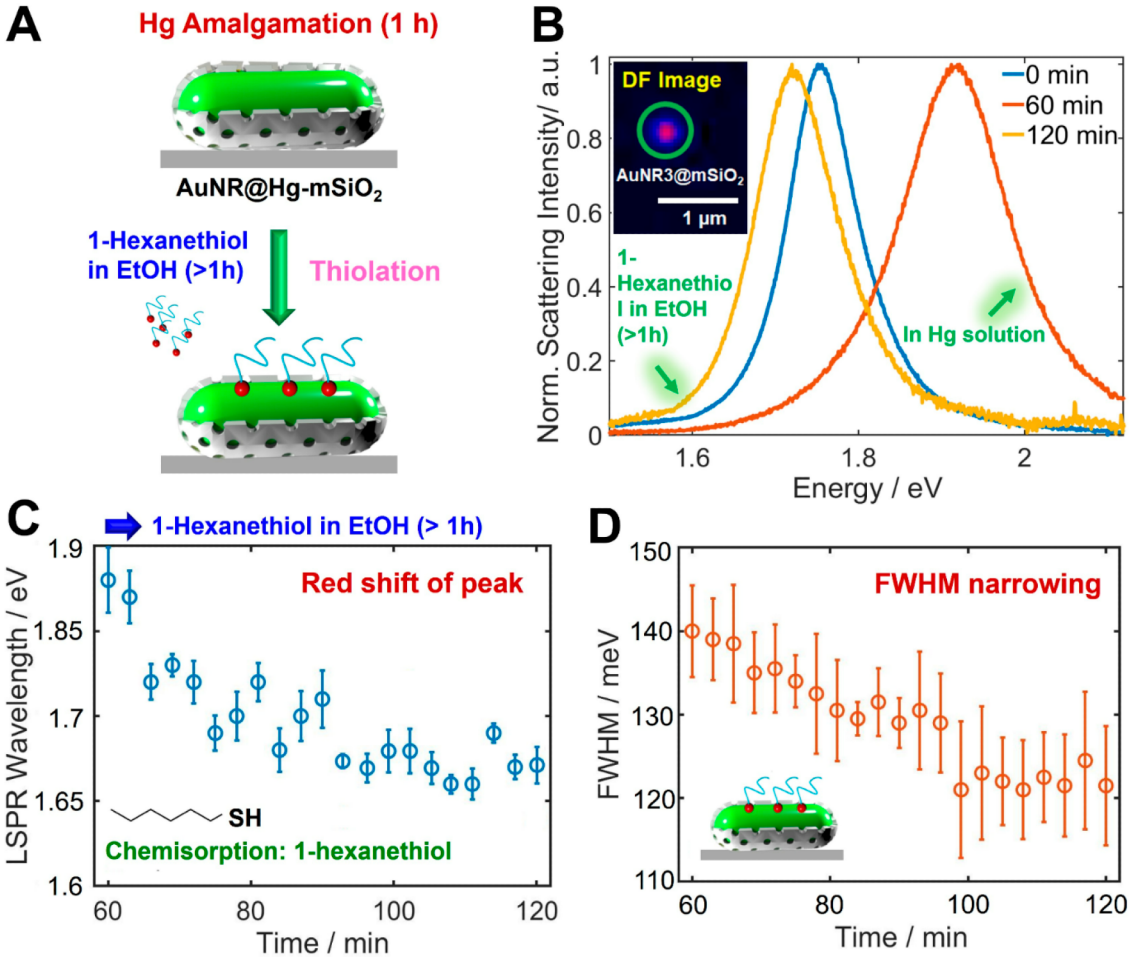

Figure 4. Effect of thiolation on the LSPR properties of single amalgamated AuNRs@$mSiO_2$. (A) Schematic representation of AuNR@Hg-$mSiO_2$ exposed to 1-hexanethiol in ethanol for chemisorption. (B) Normalized scattering spectra of AuNR3@$mSiO_2$ before exposure to Hg solution (blue curve), after exposure to Hg solution for 1 h (red curve), and after chemisorption under 1-hexanthiol (yellow curve). (C) Change in the LSPR peak of AuNRs@Hg-$mSiO_2$ exposed to 1-hexanthiol in ethanol during chemisorption as a function of time. (D) Change in the corresponding LSPR line width of AuNRs@Hg-$mSiO_2$ exposed to 1-hexanthiol in ethanol during chemisorption as a function of time.

and line width narrowing in the LSPR spectrum was observed over the course of 24 h owing to the inward Hg diffusion into the AuNR@$mSiO_2$ structure (Figure 3C and D); this was consistent with our previous study.[15] Because of the slow inward diffusion of Hg atoms into Au atoms, a solid amalgam of intermixed Au and Hg atoms may predominantly form at this stage. Consequently, the free electron density may decrease slowly as Hg diffusion progresses over 24 h, resulting in the redshift and line width narrowing in the LSPR spectrum. The LSPR spectrum obtained from AuNR2@$mSiO_2$ also supports the slow inward diffusion of Hg into the AuNR core (Figure S10).

Chemical Effect on LSPR Properties in Amalgamated AuNRs@$mSiO_2$

The chemical effect caused by adsorbate molecules on the plasmonic properties of amalgamated AuNRs@Hg-$mSiO_2$ was then analyzed and has not been studied thus far. In this study, we initially used 1-alkanethiol with a six-carbon chain (1-hexanethiol, C6) as the adsorbate to modify the chemical interfaces. The time-dependent kinetics of 1-hexanethiol adsorption on AuNRs@Hg-$mSiO_2$ were investigated. For the surface modification of AuNRs, thiol molecules have been widely used as adsorbates owing to their strong binding affinity with the Au surface via strong covalent soft−soft bonding between Au−S atoms.[32,33] Moreover, thiols have a well-known affinity for Hg and can strongly interact with soft Hg surfaces.[5,34]

After amalgam formation in Hg solution for 1 h (step 1 in Figure 1A), the amalgamated AuNRs@$mSiO_2$ were removed from the solution and exposed to 1-hexanethiol in ethanol for chemisorption, as shown in Figure 4A. We measured the single-particle scattering spectra for 2 h during exposure. More Hg and fewer Au atoms were accessible on the surface for chemisorption, owing to the Hg shell formed on the AuNR core after step 1. Figure 4B shows the single-particle spectra of amalgamated AuNR3@$mSiO_2$ (Figure S11) after incubation for 0 and 1 h in Hg solution with the 1 h Hg-treated sample incubated for another 1 h in 1-hexanethiol (120 min in Figure 4B, yellow curve). As discussed previously, 1 h of incubation in Hg solution caused Hg-shell layer formation, resulting in a blueshift and line width broadening of the LSPR peak. However, after removing the sample from the Hg solution (after 1h) and allowing it to react with 1-hexanethiol in ethanol, the spectra measured at 3 min intervals showed a gradual redshift of the LSPR peak and narrowing of the full width at half-maximum (fwhm) (Figure 4C and D). Initially, at 0 min of reaction with 1-hexanethiol (60 min in Figure 4B, red

https://doi.org/10.1021/jacsau.3c00578
JACS Au 2023, 3, 3247−3258

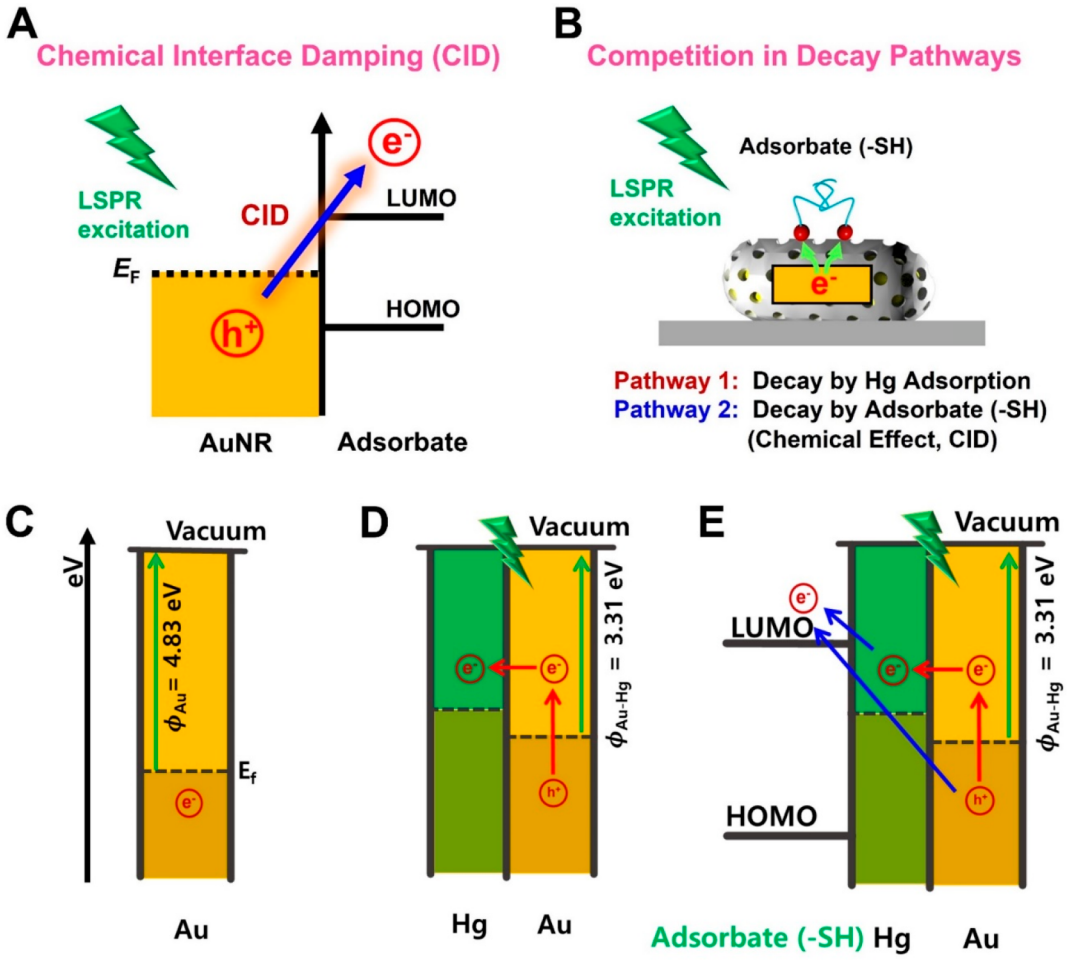

Figure 5. (A) Schematic representation of chemical interface damping (CID) induced by an adsorbate on the AuNR surface. (B) Schematic representation of the competition between the two primary decay mechanisms in single amalgamated AuNRs@mSiO$_2$. Pathway 1 is caused by Hg adsorption and coating on the AuNR core. However, in the presence of surface thiol molecules, CID can act as an additional damping pathway (pathway 2) induced by interfacial hot electron transfer from the metal to adsorbate molecules and compete with pathway 1. (C–E) Energy level diagrams for AuNRs@mSiO$_2$, amalgamated AuNRs@mSiO$_2$ (1 h), and amalgamated AuNRs@mSiO$_2$ (1 h) with the chemisorption of 1-hexanethiol in ethanol.

curve), the LSPR peak was at 1.92 eV, whereas after 1 h of reaction, the LSPR peak redshifted to 1.72 eV (yellow curve in Figure 4B). Accordingly, the LSPR line width was 153 meV at 0 min in 1-hexanethiol and decreased to 124 meV after 1 h of 1-hexanethiol chemisorption in ethanol. When the sample was exposed to air, the redshift and line width narrowing were attributed to slow inward Hg diffusion over 24 h (Figure 3). Interestingly, the chemisorption of 1-hexanethiol on the surface of amalgamated AuNR3@mSiO$_2$ promoted the line width narrowing and caused a gradual redshift of the LSPR peak within 1 h. The redshift and line width narrowing of the LSPR peak were similar in multiple amalgamated AuNR@mSiO$_2$ samples (Figure S12). Notably, the line width narrowing within 1 h of chemisorption was not caused by inward Hg diffusion into the AuNR core because core diffusion occurs with much increased time (>10 h, Figure 3). Moreover, no structural transformation was observed after 1 h of 1-hexanethiol chemisorption in ethanol on the amalgamated AuNRs@mSiO$_2$ (Figure S13). To our knowledge, this is the first report of the chemical effect on LSPR spectral changes in amalgamated AuNRs@mSiO$_2$ at the single-particle level.

Competition between Surface Plasmon Decay Pathways in Amalgamated AuNRs@mSiO$_2$

We attempted to elucidate the redshift and line width narrowing of the LSPR peak by interacting thiol molecules with the amalgamated AuNRs@mSiO$_2$, as shown in Figure 4. The LSPR peak was redshifted after the chemisorption of 1-hexanethiol on amalgamated AuNRs@mSiO$_2$ owing to an increase in the local refractive index (RI) surrounding the NPs, as illustrated in Figure 4B and C.[32] Line width narrowing in the LSPR spectrum, in contrast to the line width broadening observed upon CID of single AuNRs, was observed for the amalgamated AuNRs@mSiO$_2$. The change in electron density of amalgamated AuNRs@mSiO$_2$ continued, owing to the change in energy level due to thiol adsorption. There is a proportional relationship between the line width and damping rate in a homogeneous LSPR spectrum.[17,32] Thus, the LSPR line width narrowing is correlated with the plasmon damping rate and pathways in single AuNRs@mSiO$_2$. In this study, the competition among the surface damping pathways was examined to elucidate the chemical effects. Recently, adsorbates have been reported to provide an additional plasmon damping pathway called CID.[18,19,32,33,35] As shown in Figure 5A, closely or strongly interacting adsorbates induce

https://doi.org/10.1021/jacsau.3c00578
JACS Au 2023, 3, 3247–3258

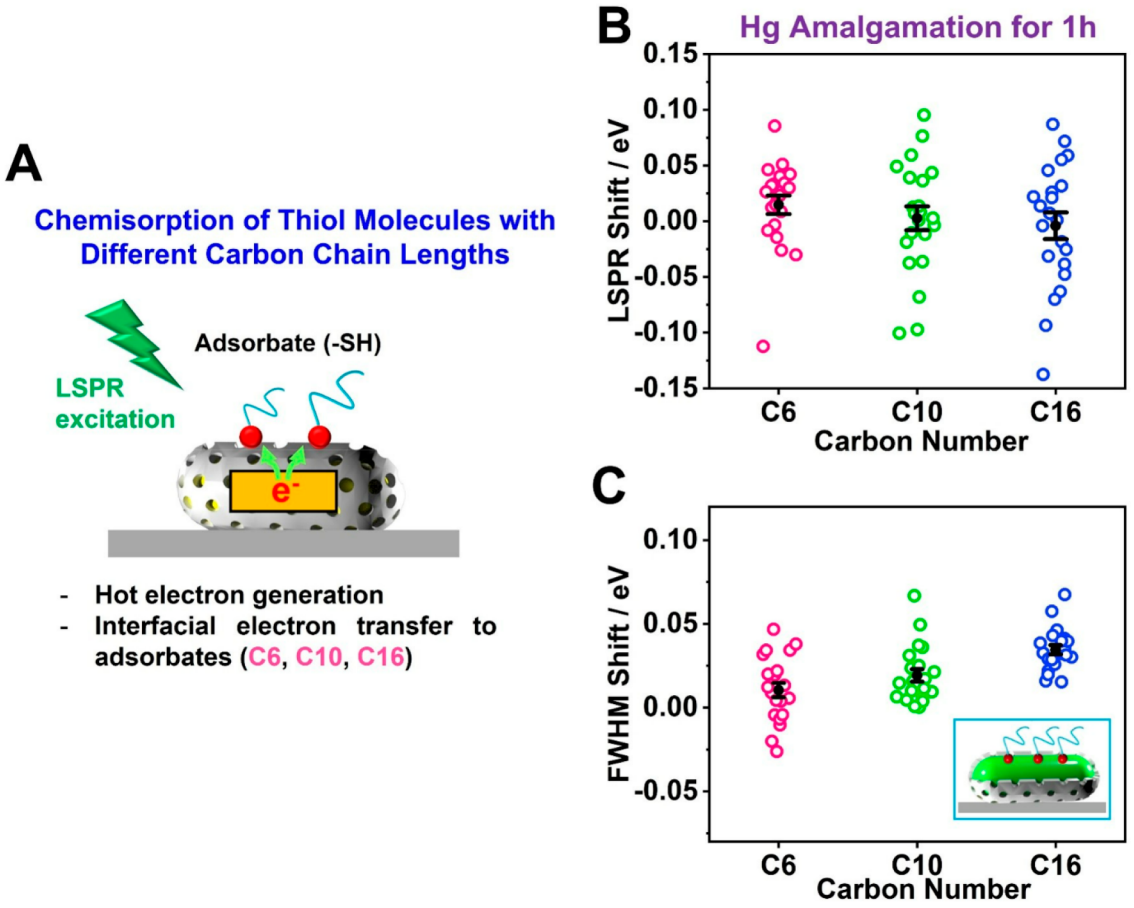

Figure 6. (A) Schematic representation of the CID effect induced by 1-alkanethiols in ethanol with three different carbon chain lengths (1-hexanethiol, C6; 1-decanethiol, C10; 1-hexadecanethiol, C16) for AuNRs@mSiO$_2$ obtained after 1 h of Hg amalgamation (step 1). (B) Comparison of the LSPR peak shifts caused by 1-alkanethiols (C6, C10, and C16), as calculated by comparing the LSPR peak energy of thiolated AuNRs@Hg-mSiO$_2$ with that of the bare AuNRs@mSiO$_2$. (C) Comparison of the corresponding fwhm shifts caused by 1-alkanethiols (C6, C10, and C16) in ethanol.

the direct generation of hot electrons for the empty lowest unoccupied molecular orbital (LUMO) of the adsorbate within 5 to 100 fs.[36−39] Accordingly, the LSPR peak is redshifted and decreases in intensity, and the line width broadens.[17,40−42] In this study, thiol chemisorption can result in another CID pathway in addition to the existing surface damping pathway induced by Hg coating on amalgamated AuNRs@mSiO$_2$. Thus, the line width narrowing in Figure 4 can be interpreted in terms of the coexistence and competition between the two surface damping pathways in a single amalgamated AuNRs@mSiO$_2$. It should be noted that the LSPR line width change can also be contributed by bulk damping, radiation damping, and electron-surface scattering in plasmonic nanomaterials. However, the above-mentioned damping mechanisms are intrinsic to plasmonic nanomaterials with specific or known sizes. In our hybrid system, due to the involvement of other metals and molecular adsorbates, it can be inferred that hot carrier generation is the predominant factor contributing to the variation in the LSPR spectral line width.[17,32,43]

As shown in Figure 5B, pathway 1 is caused by Hg coating the AuNR core or metal interface damping (MID), which broadens the LSPR line width, as shown in Figure 3. However, in the presence of surface thiol molecules, CID can also occur (pathway 2), which is induced by interfacial hot electron transfer from the metal to adsorbate molecules and can compete with pathway 1, as shown in Figure 5B. Thus, the line width narrowing in Figure 4D indicates that the considerable LSPR broadening caused by the MID (pathway 1) considerably decreases because of CID (pathway 2) upon the chemisorption of thiol molecules. Figure 5C shows the energy level diagram for AuNR@mSiO$_2$ with the calculated work function (Φ_{Au}) of 4.83 eV for Au from the XPS data by subtracting the photon energy from the binding energy of the secondary edge (slope) (Figure S14).[44] However, in the case of AuNRs@Hg-mSiO$_2$ (the core−shell structure obtained after step 1), the calculated work function for the Au−Hg core−shell structure (Φ_{Au-Hg}) decreased to 3.31 eV (Figures 5D and S15), indicating an increase in the electron density of AuNRs@Hg-mSiO$_2$ (core−shell structure) after 1 h. Although the decrease in electron density of Au was observed after the beginning of the amalgamation process (as explained in earlier sections by the Au 4f peak shifts, Figure 2A), the overall electron density of AuNRs@Hg-mSiO$_2$ (core−shell structure) increased.

When thiol molecules are chemisorbed onto AuNRs@Hg-mSiO$_2$ (the core−shell structure after step 1), the thiol will primarily interact and form a strong bond with Hg instead of with Au. Like Au, sulfur strongly bonds to Hg because S, especially S^{2-}, which is a soft base, and Hg^{2+}, which is a soft acid, interact well together.[34,45] In this case, the hot electrons generated in the Au will likely not directly transfer from Au to the LUMO of the adsorbate molecule via the CID pathway

https://doi.org/10.1021/jacsau.3c00578
JACS Au 2023, 3, 3247−3258

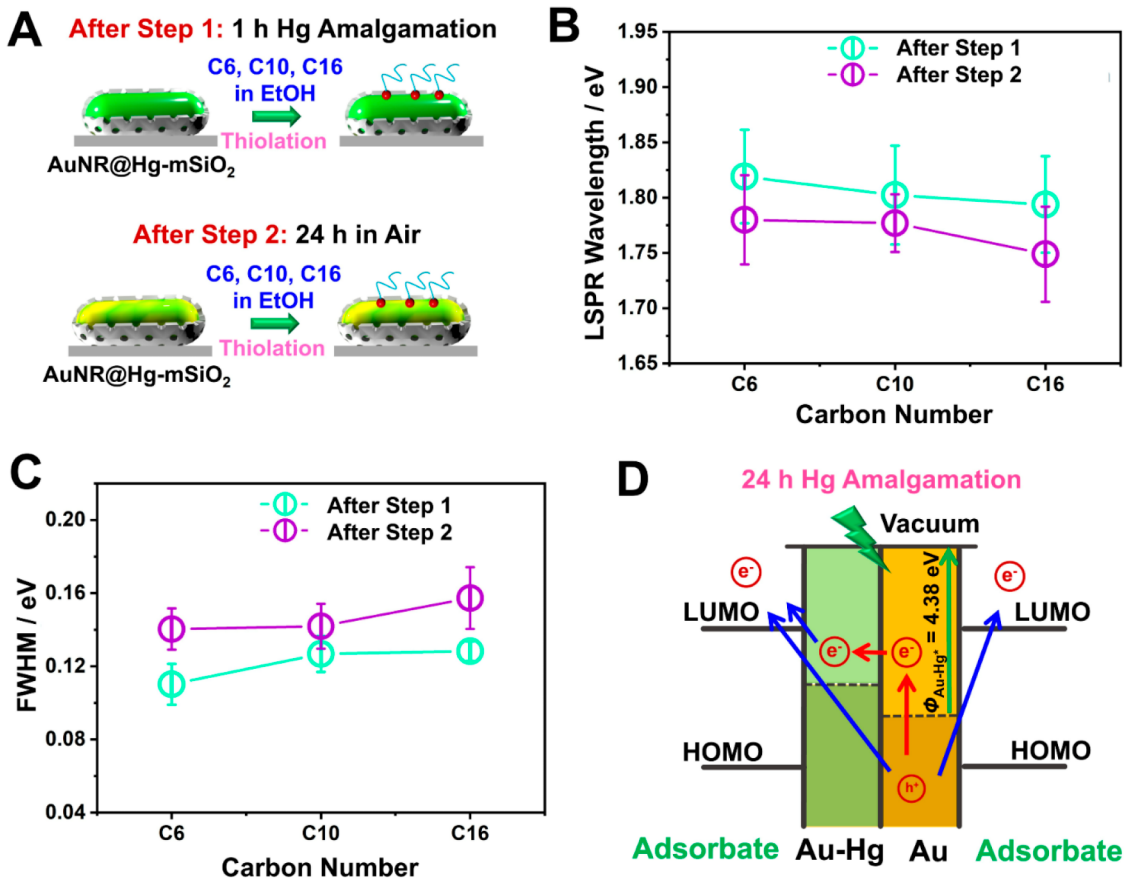

Figure 7. (A) Comparison of the CID effect induced by thiolation after step 1 (1 h of Hg amalgamation) with that after step 2 (24 h of inward Hg diffusion) in the amalgamated AuNRs@mSiO$_2$. After step 1, Hg coats the AuNR surface, producing an Au−Hg core−shell structure. However, after step 2, the coated Hg diffuses into the AuNR core to a certain degree (a few nanometers), producing a different Hg state on the AuNR surface. (B) Changes in the LSPR peak energy of AuNRs@mSiO$_2$ induced by thiolation with three different carbon lengths of 1-alkanethiols (C6, C10, and C16) after steps 1 and 2. (C) Corresponding changes in the LSPR line width of AuNRs@mSiO$_2$ induced by thiolation with three different carbon lengths after steps 1 and 2. (D) Energy level diagram of amalgamated AuNRs@Hg-mSiO$_2$ (24 h) with thiolation.

owing to the Hg shell (pathway 2, blue arrow in Figure 5E). Instead, the hot electrons in the Au will be transferred to the Hg shell first (pathway 1, red arrow in Figure 5D) via MID and then to the LUMO of the adsorbed thiol molecule via CID (pathway 2) at the Hg−thiol interface.[34] This process will decrease the overall electron transfer rate from Au to the adsorbate with a decreased plasmon damping rate, which can narrow the LSPR line width compared to that of AuNR@Hg-mSiO$_2$ without adsorbed molecules. Therefore, the results confirm that the MID (pathway 1) from Au to Hg is more dominant than the direct CID (pathway 2) from Au to the adsorbate during the competition for single amalgamated AuNRs@mSiO$_2$ after step 1 (a core−shell structure). To the best of our knowledge, this is the first study to describe the competition between CID and other surface decay channels in single plasmonic NPs.

Tuning the Interfacial Electron Transfer in Amalgamated AuNRs@mSiO$_2$

To better understand the electron transfer process (or CID) at the Hg−thiol interface and the tunability, we performed single-particle spectroscopic studies using thiol molecules with different carbon chain lengths as adsorbates. We chose 1-alkanethiols with different chain lengths because the CID process can be tuned by controlling the chemical nature of the adsorbate and the interfacial hot electron transfer from the metal to adsorbate.[32,33,35,46] In our previous studies, the LSPR line width (or CID) increased with an increasing number of linear carbons owing to increased van der Waals forces.[35,46,47] In this study, amalgamated AuNRs@mSiO$_2$ obtained after step 1 (core−shell structure) were exposed to three different 1-alkanethiols in ethanol (1-hexanethiol, 1-decanethiol, and 1-hexadecanethiol) for 1 h (Figures 6A and S16). Figure S17 shows the time-dependent changes in the LSPR peak position and line width during the Hg amalgamation and thiolation with the three different 1-alkanethiols. Figure 6B and C shows the LSPR peak and line width shifts calculated by comparing the LSPR peak energy and FHWM of the thiolated AuNRs@Hg-mSiO$_2$ with those of bare AuNRs@mSiO$_2$. The LSPR peak shift for the amalgamated AuNRs@mSiO$_2$ decreased with an increasing carbon chain length from C6 to C16, while the fwhm shift increased with an increasing chain length. The increased fwhm shift with increased chain length can be attributed to the enhanced interfacial hot electron transfer from Hg to the adsorbate via CID at the interface (Figure 5E).[35,46] Thus, CID at the Hg−thiol interface occurs, and the plasmon damping rate increases with longer chain lengths in single amalgamated AuNRs@mSiO$_2$. In addition to the CID effect, as explained earlier, the chemical-induced permittivity (CIP) effect[29] can explain the result shown in Figure 6C. The longer-chain thiols having more electrons may form slower oxidative complexation than the shorter-chain thiols because of

https://doi.org/10.1021/jacsau.3c00578
JACS Au 2023, 3, 3247−3258

their prolonged reorientation and redistribution of electrons on metal surfaces; thus, van der Waals forces increase with increasing carbon chain length.[35,48] Since the dielectric function or relative permittivity of plasmonic materials is highly dependent on the surface electron density, the adsorption of longer-chain thiol may induce a high permittivity (or CIP) and a large change in the electron density of states (DOS) at the amalgamated AuNR cores and thiol interfaces. Therefore, the chemical effect with 1-hexadecanethiol (C16) is higher than those with 1-hexanethiol (C6) and 1-decanethiol (C10); thus, the LSPR alterations caused by long carbon chain thiols are enhanced in amalgamated AuNRs@mSiO$_2$ compared with those caused by short chain thiols. To the best of our knowledge, this is the first report to describe the tunability of interfacial electron transfer (or CID) via chemisorption in amalgamated AuNRs@mSiO$_2$.

Additionally, an important point needs to be discussed with regard to Figures 4 and 6. The interfusion of Hg atoms into the AuNR cores of AuNRs@mSiO$_2$ resulted in a gradual redshift and line width narrowing in the LSPR spectrum in air compared to that in solution, as shown in Figure 3. Inward Hg diffusion is a slow process, and the redshift and line width narrowing of the LSPR peak were constant after ∼24 h.[27] In our previous study, oxygen plasma treatment resulted in faster inward diffusion of Hg into AuNR cores within 20 min.[27] Herein, when the amalgamated AuNRs@mSiO$_2$ were subjected to 1-alkanethiol, the redshift and line width narrowing of the LSPR peak saturated within 1 h. Therefore, chemical treatments can be used to tune the LSPR properties of amalgamated AuNRs@mSiO$_2$ without causing structural deformation, which has not been demonstrated previously.

Effect of the Au−Hg Surface Property on Competition between Surface Damping Pathways in Single Amalgamated AuNRs@mSiO$_2$

We then investigated the effect of the time-dependent Au−Hg surface properties on the competition between surface damping pathways in single amalgamated AuNRs@mSiO$_2$. As shown in Figure 7A, we compared the CID effect induced by thiolation after step 1 (1 h of Hg amalgamation) to that after step 2 (24 h in air) in the amalgamated AuNRs@mSiO$_2$. As explained, during step 1, at the initial stage of Hg amalgamation, the Au−Hg core−shell structure was predominant on the AuNRs@mSiO$_2$ (Figures 1A and 7A).[28] However, after step 2 (24 h in air), both Au and Hg atoms were exposed to the surface owing to inward Hg diffusion and solid amalgamation of Au−Hg over the surface. Then, we studied the competition between the two surface damping pathways in amalgamated AuNRs@mSiO$_2$ under different Au−Hg surface properties after steps 1 and 2.

Figure S18 shows the normalized scattering spectra of AuNR4@mSiO$_2$ before exposure to Hg solution (blue curve), AuNR4@mSiO$_2$ after exposure to Hg solution for 1 h (red curve), AuNR4@mSiO$_2$ after exposure to Hg in air for 24 h (yellow curve), and AuNR4@mSiO$_2$ after exposure to Hg solution and after thiolation with C6 (purple curve). Figure 7B and C shows changes in the LSPR peak and line width for AuNRs@mSiO$_2$, respectively, induced upon thiolation with three different 1-alkanethiols (C6, C10, and C16) after steps 1 and 2. Increasing the carbon chain length decreased the LSPR peak energy (or redshifted) for the AuNRs@mSiO$_2$ after steps 1 and 2. The LSPR line width broadened with increasing carbon chain length for the AuNRs@mSiO$_2$ after steps 1 and 2. However, the 24-h condition (step 2) broadened the line width more than the 1-h condition (step 1) for the same thiol carbon chain length for single AuNRs@mSiO$_2$ (Figure 7C). Because sulfur has a strong affinity toward both Au and Hg, thiol molecules will react with the Au and Hg atoms that are exposed to the surface in the single amalgamated AuNRs@mSiO$_2$ after step 2, as supported by the XPS data shown in Figure 2. Thus, the amalgamated Ag−Hg surface property strongly influences the energy and line width of the LSPR peak for single amalgamated AuNRs@mSiO$_2$.

To determine the interfacial damping that occurs in this system and the competition between the two decay pathways (Figure 5), we calculated the work function from the XPS data and compared the work function of the Au−Hg amalgam at each step in the process at 1 h (Φ_{Au-Hg}) and 24 h (Φ_{Au-Hg^*}) of Hg treatment with the work function (Φ_{Au}) of bare AuNR@mSiO$_2$. The calculated work function (Φ_{Au}) of bare AuNR@mSiO$_2$ was 4.83 eV. However, the Φ_{Au-Hg} after 1 h of Hg amalgamation decreased to 3.31 eV, and then, it increased to 4.38 eV (Figures 7D and S19) after step 2 (Φ_{Au-Hg^*}). Thus, the electron density of the AuNR core increased as the Au−Hg core−shell structure formed after step 1, and the electron density slightly decreased after step 2 as Hg amalgamation slowly intensified. For 1 h of Hg amalgamation (step 1, Figure 5E), the energetic hot electrons generated in Au are excited to Hg more easily via pathway 1 because the electron density is higher after the Hg shell formation. Therefore, pathway 1 (or MID) between Au and Hg will be dominant over pathway 2 (or CID) from Au to the adsorbate, as discussed (Figure 5). In contrast, for 24 h of Hg amalgamation (step 2, Figure 7D), the electron density decreases owing to the complete amalgam formation from the intermix of Au−Hg atoms. Notably, the unamalgamated Au core could still be available at the center of the AuNR; thus, the hot electrons generated at the core can transfer to the amalgamated Au−Hg surface via pathway 1 (MID). However, after step 2, pathway 2 (CID) will be dominant over pathway 1 (MID) owing to the availability of exposed Au and Hg atoms for thiol interactions on the surface.[45,49] Au bonds more strongly to sulfur than Hg does.[45] Thus, the stronger surface damping observed upon 24 h of treatment than for the 1-h treatment can be ascribed to the stronger interaction of Au and Hg with the − SH group. Thus, we provide new insights into CID and its competition effects for the different Au−Hg surface properties of amalgamated AuNRs@mSiO$_2$ upon adsorption of thiol molecules.

The detection of Hg^{2+} ions using plasmonic nanoparticles has been reported earlier.[1−3,6,7,11] However, a deeper understanding of plasmon damping caused by Hg amalgamation at the single-particle level is still limited.[12−16] Moreover, a complex plasmon damping mechanism involving two different pathways, namely, MID and CID, and a competition between these two damping pathways in a system at the single-particle level have not been understood earlier. Therefore, this study, providing a deeper understanding of the different stages of the Hg amalgamation process and the plasmon damping effects caused by Hg deposition as well as thiolation at the single-particle level without any noticeable structural change in AuNRs@mSiO$_2$, can be effectively utilized to design plasmonic sensors. Additional studies on plasmonic sensors using the LSPR line width of AuNRs@mSiO$_2$ to detect various adsorbate molecules are underway.

https://doi.org/10.1021/jacsau.3c00578
JACS Au 2023, 3, 3247−3258

CONCLUSIONS

In summary, we investigated Hg amalgamation without structural deformation in single AuNRs@$mSiO_2$ by using DF microscopy and spectroscopy. Hg inward diffusion into Au resulted in a blueshift of the LSPR peak and significant line width broadening. The subsequent inward Hg diffusion into the AuNR core, as confirmed by XPS, caused a gradual redshift and line width narrowing of the LSPR peak over a long time (24 h). Our investigation of the effect of the chemisorption of thiol molecules on single amalgamated AuNRs@Hg-$mSiO_2$ resulted in a redshift and line width narrowing of the LSPR peak within 1 h; in contrast, a redshift and line width broadening of the LSPR peak caused by thiolation were observed in single AuNRs in previous studies. To determine the chemical effect, the competition between the two surface decay pathways, MID and CID, was investigated. In the amalgamated AuNRs@Hg-$mSiO_2$, the CID process competed with MID, and the line width narrowing induced by thiolation indicated that the considerable LSPR broadening caused by MID decreased owing to the additional damping pathway (CID) that occurred at the interface upon the chemisorption of thiol molecules. Next, we exposed the amalgamated AuNRs@Hg-$mSiO_2$ to three different 1-alkanethiols in ethanol (1-hexanethiol, 1-decanethiol, and 1-hexadecanethiol) for 1 h. The LSPR peak shift for AuNRs@Hg-$mSiO_2$ decreased with increasing carbon chain length from C6 to C16, while the fwhm shift increased with increasing chain length. The increased fwhm shift with increasing carbon chain length can be attributed to enhanced interfacial hot electron transfer from Hg to the adsorbate via CID at the interface. Thus, these chemical treatments were demonstrated to be new, effective methods for tuning the CID and LSPR properties of amalgamated AuNRs@Hg-$mSiO_2$. Finally, we investigated the effect of the time-dependent Au−Hg surface properties on the competition between the two surface damping pathways in single AuNRs@Hg-$mSiO_2$. The 24-h Hg treatment condition led to increased line width broadening compared with the 1-h Hg treatment condition for the same thiols in the single AuNRs@Hg-$mSiO_2$. In the case of 1-h Hg treatment, the thiol molecule interacted with the Hg shell on the AuNR core, and the electron density increased in the Au−Hg core−shell structure to facilitate the transfer of energetic hot electrons from Au to Hg. Thus, pathway 1 is more dominant than pathway 2 from Au to the adsorbate. In contrast, in 24-h Hg amalgamation, because of internal Hg diffusion, the availability of exposed Au and Hg atoms over the surface, and stronger bonding of the thiol with Au and Hg, CID was dominant. Thus, the LSPR line width increased for the 24-h amalgamation owing to enhanced CID (pathway 2), as opposed to the predominance of MID (pathway 1) during the 1-h amalgamation. Therefore, this study provides new insights into Hg amalgamation without structural deformation in AuNRs@$mSiO_2$, the effect of chemical treatments, the competition between the surface damping pathways, the effect of Au−Hg surface properties on the CID, and methods for controlling the LSPR properties.

ASSOCIATED CONTENT

Supporting Information

The Supporting Information is available free of charge at https://pubs.acs.org/doi/10.1021/jacsau.3c00578.

SEM images of AuNRs@$mSiO_2$, UV−vis extinction spectrum, size distribution after Hg amalgamation, EDX mapping images of amalgamated AuNRs@$mSiO_2$, photograph of the experimental setup, single-particle spectra to show the chemical effects after using three different 1-alkanethiols (different carbon chain lengths) as adsorbates (PDF)

AUTHOR INFORMATION

Corresponding Author

Ji Won Ha − *Department of Chemistry, University of Ulsan, Nam-gu, Ulsan 44610, South Korea; Energy Harvest-Storage Research Center (EHSRC), University of Ulsan, Nam-gu, Ulsan 44610, South Korea;* orcid.org/0000-0003-0566-8176; Phone: +82-52-712-8012; Email: jwha77@ulsan.ac.kr; Fax: +82-52-712-8002

Authors

Yola Yolanda Alizar − *Department of Chemistry, University of Ulsan, Nam-gu, Ulsan 44610, South Korea*

Mukunthan Ramasamy − *Energy Harvest-Storage Research Center (EHSRC), University of Ulsan, Nam-gu, Ulsan 44610, South Korea;* orcid.org/0000-0003-4402-8649

Geun Wan Kim − *Department of Chemistry, University of Ulsan, Nam-gu, Ulsan 44610, South Korea*

Complete contact information is available at: https://pubs.acs.org/10.1021/jacsau.3c00578

Notes

The authors declare no competing financial interest.

ACKNOWLEDGMENTS

This work was supported by two National Research Foundation of Korea (NRF) grants funded by the Korean government (MSIP) (Nos. RS-2023-00208346 and 2019R1A6A1A11053838).

REFERENCES

(1) Verma, M. S.; Chandra, M. Nonlinear plasmonic sensing for label-free and selective detection of mercury at picomolar level. *ACS Sens.* **2020**, *5*, 645−649.

(2) Senapati, T.; Senapati, D.; Singh, A. K.; Fan, Z.; Kanchanapally, R.; Ray, P. C. Highly selective SERS probe for Hg(ii) detection using tryptophan-protected popcorn shaped gold nanoparticles. *Chem. Commun.* **2011**, *47*, 10326−10328.

(3) Ojea-Jiménez, I.; López, X.; Arbiol, J.; Puntes, V. Citrate-coated gold nanoparticles as smart scavengers for mercury(II) removal from polluted waters. *ACS Nano* **2012**, *6*, 2253−2260.

(4) Kim, G. W.; Ha, J. W. Influence of mercury amalgamation on three-dimensional orientation of single gold nanorods coated with mesoporous silica shell. *Bull. Korean Chem. Soc.* **2022**, *43*, 1040−1044.

(5) Zheng, W.; Lin, H.; Mann, B. F.; Liang, L.; Gu, B. Oxidation of dissolved elemental mercury by thiol compounds under anoxic conditions. *Environ. Sci. Technol.* **2013**, *47*, 12827−12834.

(6) Zhao, Q.; Zhang, H.; Fu, H.; Wei, Y.; Cai, W. Raman reporter-assisted Au nanorod arrays SERS nanoprobe for ultrasensitive detection of mercuric ion (Hg2+) with superior anti-interference performances. *J. Hazard. Mater.* **2020**, *398*, 122890.

(7) Liu, X.; Huang, D.; Lai, C.; Zhang, C.; Qin, L.; Li, B.; Yi, H.; Deng, R.; Liu, S.; Zhang, M.; Lei, L.; Fu, Y.; Li, L. Visual method for selective detection of Hg2+ based on the competitive interactions of 2-thiobarbituric acid with Au nanoparticles and Hg2+. *ACS Appl. Nano Mater.* **2021**, *4*, 6760−6767.

(8) Xu, D.; Yu, S.; Yin, Y.; Wang, S.; Lin, Q.; Yuan, Z. Sensitive colorimetric Hg2+ detection via amalgamation-mediated shape transition of gold nanostars. *Front. Chem.* **2018**, *6*, 566.
(9) Logan, N.; Lou-Franco, J.; Elliott, C.; Cao, C. Catalytic gold nanostars for SERS-based detection of mercury ions (Hg2+) with inverse sensitivity. *Environ. Sci. Nano* **2021**, *8*, 2718−2730.
(10) Song, Y.; Bai, J.; Zhang, R.; Wu, E.; Wang, J.; Li, S.; Ning, B.; Wang, M.; Gao, Z.; Peng, Y. LSPR-enhanced photonic crystal allows ultrasensitive and label-free detection of hazardous chemicals. *Sens. Actuators B Chem.* **2020**, *310*, 127671.
(11) Schopf, C.; Martin, A.; Iacopino, D. Plasmonic detection of mercury via amalgam formation on surface-immobilized single Au nanorods. *Sci. Technol. Adv. Mater.* **2017**, *18*, 60−67.
(12) Schopf, C.; Martín, A.; Schmidt, M.; Iacopino, D. Investigation of Au-Hg amalgam formation on substrate-immobilized individual Au nanorods. *J. Mater. Chem. C* **2015**, *3*, 8865−8872.
(13) Lee, J.; Kim, G. W.; Ha, J. W. Single-particle study: effects of mercury amalgamation on morphological and spectral changes in anisotropic gold nanorods. *Analyst* **2022**, *147*, 1066−1070.
(14) Mertens, S. F. L.; Gara, M.; Sologubenko, A. S.; Mayer, J.; Szidat, S.; Kramer, K. W.; Jacob, T.; Schiffrin, D. J.; Wandlowski, T. Au@Hg nanoalloy formation through direct amalgamation: structural, spectroscopic, and computational evidence for slow nanoscale diffusion. *Adv. Funct. Mater.* **2011**, *21*, 3259−3267.
(15) Kim, G. W.; Ha, J. W. Single-particle study on Hg amalgamation mechanism and slow inward diffusion in mesoporous silica-coated gold nanorods without structural deformation. *J. Phys. Chem. Lett.* **2022**, *13*, 2607−2613.
(16) Alizar, Y. Y.; Ha, J. W. Single-particle spectroelectrochemistry: electrochemical tuning of plasmonic properties via mercury amalgamation in mesoporous silica coated gold nanorods without structural deformation. *Analyst* **2022**, *147*, 2035−2039.
(17) Foerster, B.; Joplin, A.; Kaefer, K.; Celiksoy, S.; Link, S.; Sönnichsen, C. Chemical interface damping depends on electrons reaching the surface. *ACS Nano* **2017**, *11*, 2886−2893.
(18) Heo, S. E.; Ha, J. W. Single-particle correlation study: chemical interface damping in gold nanorods coated with mesoporous silica shell. *Bull. Korean Chem. Soc.* **2022**, *43*, 797−800.
(19) Ryu, K. R.; Ha, J. W. Chemical interface damping of silver-coated gold nanorods using supramolecular host-guest chemistry. *Bull. Korean Chem. Soc.* **2021**, *42*, 1082−1084.
(20) Hong, Y. A.; Ha, J. W. In situ reversible tuning of chemical interface damping in mesoporous silica-coated gold nanorods via direct adsorption and removal of thiol. *Analyst* **2023**, *148*, 3719−3723.
(21) Therrien, A. J.; Kale, M. J.; Yuan, L.; Zhang, C.; Halas, N. J.; Christopher, P. Impact of chemical interface damping on surface plasmon dephasing. *Faraday Discuss.* **2019**, *214*, 59−72.
(22) Lee, J.; Ha, J. W. Effects of amine linkers with different carbon chain lengths at guanine-rich polynucleotides on chemical interface damping in single gold nanorods. *Anal. Chem.* **2022**, *94*, 7100−7106.
(23) Ramasamy, M.; Ha, J. W. Single-particle spectroelectrochemistry: electrochemical approaches for tuning chemical interfaces and plasmon damping in single gold nanorods. *J. Phys. Chem. Lett.* **2023**, *14*, 5768−5775.
(24) Chen, K.; Lin, C.-C.; Vela, J.; Fang, N. Multishell Au/Ag/SiO2 nanorods with tunable optical properties as single particle orientation and rotational tracking probes. *Anal. Chem.* **2015**, *87*, 4096−4099.
(25) Rex, M.; Hernandez, F. E.; Campiglia, A. D. Pushing the limits of mercury sensors with gold nanorods. *Anal. Chem.* **2006**, *78*, 445−451.
(26) Qi, W.; Wang, Y.; Wang, J.; Huang, C. Light scattering investigations on mercury ion induced amalgamation of gold nanoparticles in aqueous medium. *Sci. China Chem.* **2012**, *55*, 1445−1450.
(27) Alizar, Y. Y.; Ramasamy, M.; Ha, J. W. Tuning plasmonic properties by promoting the inward Hg diffusion via oxygen plasma treatment in gold nanorods coated with a mesoporous silica shell. *Analyst* **2022**, *147*, 3623−3627.
(28) Wang, N.; Liu, G.; Dai, H.; Ma, H.; Lin, M. Spectroscopic evidence for electrochemical effect of mercury ions on gold nanoparticles. *Anal. Chim. Acta* **2019**, *1062*, 140−146.
(29) Saito, N.; Ryuzaki, S.; Tsuji, Y.; Noguchi, Y.; Matsuda, R.; Wang, P.; Tanaka, D.; Arima, Y.; Okamoto, K.; Yoshizawa, K.; Tamada, K. Effect of chemically induced permittivity changes on the plasmonic properties of metal nanoparticles. *Commun. Mater.* **2021**, *2*, 54.
(30) Sannomiya, T.; Dermutz, H.; Hafner, C.; Vörös, J.; Dahlin, A. B. Electrochemistry on a localized surface plasmon resonance sensor. *Langmuir* **2010**, *26*, 7619−7626.
(31) Sánchez-Iglesias, A.; Carbó-Argibay, E.; Glaria, A.; Rodríguez-González, B.; Pérez-Juste, J.; Pastoriza-Santos, I.; Liz-Marzán, L. M. Rapid epitaxial growth of Ag on Au nanoparticles: from Au nanorods to core-shell Au@Ag octahedrons. *Chem.—Eur. J.* **2010**, *16*, 5558−5563.
(32) Lee, S. Y.; Tsalu, P. V.; Kim, G. W.; Seo, M. J.; Hong, J. W.; Ha, J. W. Tuning chemical interface damping: interfacial electronic effects of adsorbate molecules and sharp tips of single gold bipyramids. *Nano Lett.* **2019**, *19*, 2568−2574.
(33) Jeon, H. B.; Park, S.; Ryu, K. R.; Ghosh, S. K.; Jung, J.; Park, K. M.; Ha, J. W. In situ reversible tuning of chemical interface damping in single gold nanorod-based recyclable platforms through manipulation of supramolecular host-guest interactions. *Chem. Sci.* **2021**, *12*, 7115−7124.
(34) Muskal, N.; Mandler, D. Thiol self-assembled monolayers on mercury surfaces: the adsorption and electrochemistry of ω-mercaptoalkanoic acids. *Electrochim. Acta* **1999**, *45*, 537−548.
(35) Lee, S. A.; Link, S. Chemical interface damping of surface plasmon resonances. *Acc. Chem. Res.* **2021**, *54*, 1950−1960.
(36) Kale, M. J.; Avanesian, T.; Christopher, P. Direct photocatalysis by plasmonic nanostructures. *ACS Catal.* **2014**, *4*, 116−128.
(37) Boerigter, C.; Campana, R.; Morabito, M.; Linic, S. Evidence and implications of direct charge excitation as the dominant mechanism in plasmon-mediated photocatalysis. *Nature Commun.* **2016**, *7*, 10545.
(38) Boerigter, C.; Aslam, U.; Linic, S. Mechanism of Charge Transfer from Plasmonic Nanostructures to Chemically Attached Materials. *ACS Nano* **2016**, *10*, 6108−6115.
(39) Seo, M. J.; Kim, G. W.; Tsalu, P. V.; Moon, S. W.; Ha, J. W. Role of chemical interface damping for tuning chemical enhancement in resonance surface-enhanced Raman scattering of plasmonic gold nanorods. *Nanoscale Horiz.* **2020**, *5*, 345−349.
(40) Chen, T.; Dong, B.; Chen, K.; Zhao, F.; Cheng, X.; Ma, C.; Lee, S.; Zhang, P.; Kang, S. H.; Ha, J. W.; Xu, W.; Fang, N. Optical super-resolution imaging of surface reactions. *Chem. Rev.* **2017**, *117*, 7510−7537.
(41) Zijlstra, P.; Paulo, P. M. R.; Orrit, M. Optical detection of single non-absorbing molecules using the surface plasmon resonance of a gold nanorod. *Nat. Nanotechnol.* **2012**, *7*, 379.
(42) Lünskens, T.; von Weber, A.; Jakob, M.; Lelaidier, T.; Kartouzian, A.; Heiz, U. Effect of thiol-ligands on the optical response of supported silver clusters. *J. Phys. Chem. C* **2017**, *121*, 9331−9336.
(43) Li, S.; Huang, H.; Shao, L.; Wang, J. How to utilize excited plasmon energy efficiently. *ACS Nano* **2021**, *15*, 10759−10768.
(44) Kim, J. W.; Kim, A. Absolute work function measurement by using photoelectron spectroscopy. *Curr. Appl. Phys.* **2021**, *31*, 52−59.
(45) Kraka, E.; Filatov, M.; Cremer, D. Comparison of gold bonding with mercury bonding. *Croat. Chem. Acta* **2009**, *82*, 233−243.
(46) Lee, S. Y.; Ha, J. W. Effect of linear chain lengths of 1-alkanethiols on plasmon damping of single gold bipyramids with sharp tips. *Bull. Korean Chem. Soc.* **2019**, *40*, 481−482.
(47) Moon, S. W.; Tsalu, P. V.; Ha, J. W. Single particle study: size and chemical effects on plasmon damping at the interface between adsorbate and anisotropic gold nanorods. *Phys. Chem. Chem. Phys.* **2018**, *20*, 22197−22202.
(48) Mete, E.; Yılmaz, A.; Danışman, M. F. A van der Waals density functional investigation of carboranethiol self-assembled monolayers on Au(111). *Phys. Chem. Chem. Phys.* **2016**, *18*, 12920−12927.

https://doi.org/10.1021/jacsau.3c00578
JACS Au 2023, 3, 3247−3258

(49) Firmanti, M. I.; Ha, J. W. Elucidating surface plasmon damping and fano resonance induced by epitaxial growth of palladium on single gold nanorods. *J. Phys. Chem. Lett.* **2023**, *14*, 8016−8023.

https://doi.org/10.1021/jacsau.3c00578
JACS Au 2023, 3, 3247−3258